Dynamic mooring simulation with *Code_Aster* with application to a floating wind turbine

Raffaello Antonutti [a,b,*], Christophe Peyrard [a,b], Atilla Incecik [c,f], David Ingram [d,f], Lars Johanning [e,f]

[a] *EDF R&D - Electricité de France Research and Development, 6 Quai Watier, 78400 Chatou, France*
[b] *Saint-Venant Hydraulics Laboratory (EDF R&D, ENPC, CEREMA), 6 Quai Watier, 78400 Chatou, France*
[c] *Department of Naval Architecture, Ocean and Marine Engineering, University of Strathclyde, Glasgow G4 0LZ, UK*
[d] *Institute for Energy Systems, School of Engineering, The University of Edinburgh, King's Buildings, Edinburgh EH9 3JL, UK*
[e] *College of Engineering, Mathematics and Physical Science, Renewable Energy Research Group, University of Exeter, Penryn Campus, Penryn TR10 9EZ, UK*
[f] *Industrial Doctoral Centre for Offshore Renewable Energy, The University of Edinburgh, King's Buildings, Edinburgh EH9 3JL, UK*

ARTICLE INFO

ABSTRACT

The design of reliable station-keeping systems for permanent floating structures such as offshore renewable energy devices is vital to their lifelong integrity. In highly dynamic and/or deep-water applications, including hydrodynamics and structural dynamics in the mooring analysis is paramount for the accurate prediction of the loading on the lines and hence their dimensioning. This article presents a new workflow based on EDF R&D's open-source, finite-element analysis tool *Code_Aster*, enabling the dynamic analysis of catenary mooring systems, with application to a floating wind turbine concept. The University of Maine DeepCwind-OC4 basin test campaign is used for validation, showing that *Code_Aster* can satisfactorily predict the fairlead tensions in both regular and irregular waves. In the latter case, all of the three main spectral components of tension observed in the experiments are found numerically. Also, the dynamic line tension is systematically compared with that provided by the classic quasi-static approach, thereby confirming its limitations. Robust dynamic simulation of catenary moorings is shown to be possible using this generalist finite-element software, provided that the inputs be organised consistently with the physics of offshore hydromechanics.

1. Introduction

Floating wind turbine (FWT) technology permits to access deep-water offshore wind resources up to depths of a few hundred metres. Whilst it has already been demonstrated at the MW scale through a handful of prototypes, its industrialisation is just beginning. Considerable challenges lie ahead due to the limited experience available in coupling a wind turbine generator to a floating structure. Producing cost-effective, integrated FWT designs will likely require a profound revision of engineering practices and quite possibly the adoption of radically innovative solutions before standardisation.

1.1. Mooring system

The station keeping of a FWT is achieved by transferring the mean horizontal loads, dominated by wind thrust, to the seabed. The mooring system, defined as the ensemble of components involved in the load path from the fairleads to the soil, must be designed to resist cyclical and extreme loads with adequate safety and, if required, redundancy. For a general introduction to offshore mooring systems and their functions, design, and certification, the reader may refer to Chakrabarti (2005).

Offshore mooring systems commonly use the catenary principle (Fig. 1a) to produce horizontal restoring forces, exploiting the gravitational potential of heavy suspended lines. On the contrary, the restoring power of taut mooring arrangements (Fig. 1b) relies primarily on their elasticity. In FWT applications, the choice of mooring solution is primarily linked to water depth and floater technology and deeply impacts system design, as well as marine operations and the risk structure of a project.

Whilst the MW-scale FWT prototypes installed to date (Hywind, WindFloat, and the units installed off Goto and Fukushima) employ slack chain moorings, semi-taut, taut or tensioned arrangements are also
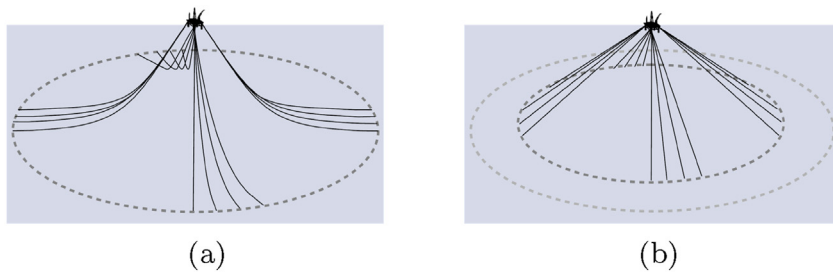
Fig. 1. Catenary (a) and taut (b) mooring arrangement a classic offshore platform, after Vryhof (2010).

considered for upcoming floating wind applications (Castro-Santos et al., 2013). Examples of taut mooring solutions using mainly fibre rope are found for instance within the early DCNS Sea Reed design and the IDEOL Floatgen demonstrator. In these cases nylon has been favoured over other fibres in order to insure sufficiently soft behaviour in very shallow water (30–40 m), where conventional arrangements become too stiff. Other configurations tailored for mid-shallow waters have been studied, such as catenary with clump weights (e.g. Vertiwind concept) or the multi-node GustoMSC patented system (de Boom, 2011). Turbine weathervaning by mooring design may eliminate the need for an active nacelle yawing system and/or attenuate loads on the floater; for this sake, single-point FWT mooring systems have been devised using a turret (e.g. Eolink and SAITEC concepts) or single anchor leg moorings. Finally, tensioned systems have been investigated in order to reduce stability demand on the floater, leading to the design of the SBM, Glosten PelaStar, and GICON tension-leg platform systems.

As imaginable, the properties of the mooring system define the dynamic response features of the whole system. Appropriately stiff or compliant behaviour in different degrees of freedom, as well as the avoidance of resonance, can be obtained by intervening on the mooring arrangement. The design of a floating wind farm mooring system that is low-maintenance, sufficiently reliable, and optimised for cost challenges the existing practices and holds large potential for improvement by R&D. Considering that a permanent floating structure's very survivability depends on the integrity of its moorings, a thorough understanding of their mechanical behaviour in the highly dynamic conditions found offshore is fundamental.

1.2. Numerical modelling of floating wind turbine moorings

In the floating offshore structure industry both frequency- and time-domain numerical tools are used for the estimate of platform and (mostly platform-driven) mooring response. The less computationally intensive frequency-domain methods treat wave-frequency and low-frequency wave loads and responses separately, typically employing linear and quadratic wave force transfer functions (QTF) to define the excitation term of the platform's rigid-body EoM (equations of motion). This approach, valid when non-linearities other than those treated with QTF are modest, is commonly applied to conventional offshore structures, especially in early design stages and for large design load case (DLC) sets (notably fatigue).

In floating wind, the addition of wind and turbine-related excitation at its own range of frequencies as well as the non-linearities caused by the reduced size of structures calls for time-domain solvers at earlier design stages. In this case all physics can be treated at once in coupled fashion albeit at higher computational cost. Concerning the effect of the mooring system on platform motions, in frequency versus time-domain (dynamic mooring) model comparisons it is common to observe relative conservatism in frequency domain results, due to absence of mooring damping (cf. for example Stendal (2015)). Conversely, mooring tensions may be underestimated by frequency-domain solvers as they typically miss line-bound inertial and hydrodynamic effects, as discussed below.

After half a century of offshore engineering experience, the role of dynamics in the mechanical behaviour of mooring systems is vastly documented. It is commonly accepted that the quasi-static representation of mooring lines becomes too inaccurate for the sake of engineering design when the motions of the structure are highly dynamic, when drag-intensive components are used (for instance, a mooring chain), when water depth exceeds about 150 m, or with any combination of the above (Matha et al., 2011). In such cases the inertial, hydrodynamic, and seabed contact loads can govern the extreme and cyclical tension regimes on the lines. Dynamic effects can dominate the tension variance especially in domains where high energy and high compliance coexist. This typically applies to conventional deep-water offshore platforms (Mavrakos et al., 1996) and to highly dynamic applications such as marine renewable energy installations (Johanning et al., 2007). As a consequence, the current state-of-the-art time-domain software for the design and analysis of offshore mooring systems (e.g. OrcaFlex, aNySIM, Flexcom, FASTlink,[1] etc.) typically include dynamic simulation capabilities.

The above guidelines are readily transposed to the floating wind context and dictate the use of dynamic simulation tools, especially when focussing on the mechanical response of the mooring system. Past research (see for example Karimirad, 2013) has shown that the dynamic mooring effects tend to bear a limited impact on FWT motion, due to the economical limitations to the practicable water depth – presently a few hundred metres at the most. Yet even in these conditions the impact on platform motion may become observable in extreme sea states, as pointed out by Masciola et al. (2013). Increasing the water depth rapidly augments the sensitivity of platform motion to the mooring dynamics, as reported by Matha et al. (2011). For instance, a lumped-mass model is used by Lin (2015) to simulate the dynamics of a spar FWT with catenary chains, for increasing water depths (320, 600, and 900 m), confirming the growing importance of dynamic line tension in determining the global response. A different picture can be drawn for the dynamic effects on mooring line tension: among others, Coulling et al. (2013) and Masciola et al. (2013) demonstrate that the quasi-static tensions severely underestimate experimental measurements even at the limited depth of 200 m and for operational met-ocean conditions.

A recent review of the available dynamic mooring line theories is provided by Masciola et al. (2014), distinguishing three main categories: lumped-mass, finite-difference, and finite-element. Literature shows that both the popular finite-element and lumped-mass theories can provide accurate tension predictions, although with more stringent resolution requirements by the latter approach (Lin, 2015; Masciola et al., 2014).

The finite-element (FE) method has been chosen by numerous authors in the FWT modelling field. A study by Jeon et al. (2013) evaluates the response of a spar-type FWT using a catenary system, evidencing the extensional vibrations of the mooring lines. The dynamics of large multi-turbine platforms are analysed by Kallesoe et al. (2011) and by Kim et al. (2015) incorporating a FE moorings model. Finite bar-type elements are used in the coupled simulations of Cheng et al. (2015) to assess different VAWT arrangements, and by Bachynski et al. (2013) to determine the severity of transient, fault-related events on mooring tension. Coupled motion response and dynamic mooring tensions are obtained by Zhang et al. (2013) for a MW-sized HAWT on a small semi-submersible

---

[1] A simulator coupling NREL's code FAST and OrcaFlex.

platform, also using the FE method. The global effect of the hydrodynamic damping forces exerted on the mooring lines is characterised in the work of Hall et al. (2011) for a spar FWT using a nonlinear bar model. A tension-leg system is also studied with the FE approach by Bae and Kim (2013), allowing to bring out the effects of 2nd order sum-frequency wave excitation on structural response. The outputs of coupled simulation software using a range of different mooring theories are benchmarked in a report by Jonkman et al. (2010).

A promising alternative for the representation of mooring dynamics is the multi-body formulation, as maintained by Borg et al. (2012) and Muskulus (2011), which may enable a reduction of computational effort compared to FE resolutions. For example, Matha et al. (2011) use this modelling option to show the onset of hydrodynamic non-linearities in the behaviour of a FWT due to mooring dynamics.

1.3. Code_Aster

Code_Aster is EDF R&D's all-purpose open-source FE solver for the thermo-mechanical study of structures (EDF, 2014). After over 20 years of development, this software offers in the order of 400 finite element typologies for the discretisation of solids and a broad range of solvers, all features which are thoroughly tested and validated. It enables the static, dynamic, and vibrational analysis of mechanically loaded structures as well as modal analysis.

The current study looks to employ the nonlinear capabilities of this software to represent the dynamic behaviour of floating wind turbine mooring lines, which are intrinsically characterised by nonlinear kinematics due to the presence of large displacements and intermittent seabed contact. The features peculiar of mooring system modelling which are not readily available in the classic *Code_Aster* workflow have been implemented by manually augmenting the command file with the necessary scripts, and by developing practical methodologies based on appropriate sequences of simulations.

Although *Code_Aster* is written in French language, the interested anglophone reader can acquire a grip on this software by consulting specialised wiki pages which provide examples and tutorials (see for instance CAELinux, 2015). Two related manuscripts have also been recently published which are rich in hands-on examples (Thakore, 2014a, b).

The version of the software employed for this study is 12.2.10 (development release).

1.4. DeepCwind-OC4 experimental campaign

An experimental campaign led by the University of Maine was conducted at MARIN's wind and wave basin with the aim of calibrating and validating a coupled FWT dynamic simulator based on NREL's FAST. Its outcomes are documented by published work by Masciola et al. (2013) and Coulling et al. (2013), where the outputs of different numerical implementations are compared to the measurements. Other authors have recently utilised this campaign for validation, using both the FE (Koo et al., 2014) and lumped-mass (Hall and Goupee, 2015) simulation approaches.

The object of this campaign is a 1/50th-scale model of the DeepCwind-OC4 FWT (Fig. 2), which consists in a scaled NREL 5 MW aerogenerator mounted on a three-column semi-submersible platform, operating at an equivalent water depth of 200 m. Included in the physical model is a downscaled mooring system, realised with a brass chain, which closely resembles the full-scale three-leg arrangement specified in Robertson et al. (2014). Load cells mounted at the fairleads provide the mooring tension signal. The experiments carried out at the MARIN facility include free-decay, pull-out, wind-only, wave-only, and coupled wind-wave tests; the numerical model benchmarks clearly exhibit the limitations of the quasi-static mooring model when it comes to assessing the dynamic tension ranges.
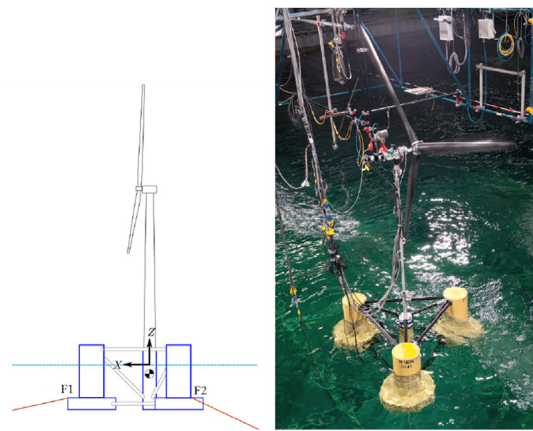

Fig. 2. Sketch of the DeepCwind-OC4 floating wind turbine (left) and a picture of the model under the action of wind and waves (right). Reproduced from Masciola et al. (2013) and Coulling et al. (2013).

1.5. Selected validation data

A subset of the experiments introduced in 1.4 is here used to validate the presented dynamic simulator. Published mooring tensions in Coulling et al. (2013) only treat purely hydrodynamic load cases, with turbine parked and no wind. For the sake of progressive model validation, the same environmental conditions are applied in this work as a first step; full environments including wind and turbine operational loads will be part of future work, with verification possibly starting from a benchmark versus comparable tools such as NREL FAST v8 (using MoorDyn) and validation from the comparison with further experimental outputs presented in Goupee et al. (2014).

2. Methodology

The finite-element method enables the spatial discretisation of a continuum, reducing the degrees of freedom (DoF) of a solid to a finite set which can be treated numerically. A corresponding set of equations written with respect to the system's nodal DoF is then used to seek the static or dynamic equilibrium configuration of the structure, under any given combination of external loads and constraints.

2.1. One-dimensional discretisation

The centrepiece of the proposed methodology is the homogeneous, 1D finite element denoted 'CABLE' available in *Code_Aster*, which was originally developed to simulate the mechanical behaviour of overhead electrical lines (Fléjou, 2014). This two-node element is a version of the classic 'bar' element, adapted to the large displacement context; this makes it suitable for representing highly compliant mooring lines.

As discussed above, bars are only one of many modelling possibilities: a simpler and widespread option for dynamic mooring modelling is the lumped mass with spring and damper connections, which requires higher mesh resolution. Whether this approach can be successfully implemented in *Code_Aster* remains to be investigated. On the opposite side, the next FE type in terms of complexity is the beam. Large-displacement beams are available in *Code_Aster* – which may be used to model mooring lines characterised by significant bending, torsional, or shear resistance – but have been shown to be prone to error accumulation when undergoing repeated large rotations. They also prove overcomplex when the mooring line's dominant mechanical resistance is axial: a beneficial feature of bar elements with respect to beams is in fact the halving of the global DoF at the nodes (rotational DoF are unassigned) which preserves computational efficiency.

It should be noted that the absence of rotational reactions which characterises the CABLE is a reasonable modelling hypothesis only for

line types which oppose negligible resistance to bending and torsion. Whilst this is generally accepted for chains (Orcina, 2013), the behaviour of less flexible lines operating at low tension such as short and stiff rope segments may not be accurately represented under this assumption, especially in the vicinity of rotational constraints. Focussing on bending and assuming a linear isotropic material and a constant line section, the classic beam theory provides the governing parameter which if large enough causes elastic behaviour, the segment's relative bending stiffness EI/L. This is defined by the material's Young's modulus E, the sectional bending inertia I, and the characteristic length of the segment L. In presence of a low (homogeneous) tension T, this term may no longer be marginal with respect to the contribution of geometric bending stiffness, which is proportional to TL and usually dominant in the reactive balance of a tensioned mooring line. The underlying assumption of bending-soft segments may be then written as $EI/L \ll TL$.

2.1.1. Finite-element constitution

A CABLE finite element is defined as a straight segment of length l with a constant cross section of area A. The element's sections are supposed to be undeformable and to maintain a constant orientation in the local frame. Used in 3D space, a CABLE disposes of six nodal DoF in the global inertial system of reference, which correspond to the nodal translations $\mathbf{q}_e = [\mathbf{q}_n^1; \mathbf{q}_n^2]$ (Fig. 3). Linear shape functions $\mathbf{L}$ are used to express the internal displacement vector $\tilde{\mathbf{u}}$ in the global frame as a function of the normalised axial position on the element, $\xi = \tilde{s}/l$, as

$$\tilde{\mathbf{u}}(\xi) = \mathbf{L}\mathbf{q}_e, \tag{1}$$

using

$$\mathbf{L} = \begin{bmatrix} 1-\xi & 0 & 0 & \xi & 0 & 0 \\ 0 & 1-\xi & 0 & 0 & \xi & 0 \\ 0 & 0 & 1-\xi & 0 & 0 & \xi \end{bmatrix}. \tag{2}$$

The mechanical tensors describing a system of interconnected cables can be obtained by applying the Lagrange equations and hence assembling the DoF-matched individual element contributions. No basis changes are necessary thanks to the purely translational constitution of this element type, which allows to write the kinematics directly in the common global frame.

2.2. Large displacements

The presence of large displacements, whether due to deformation or rigid-body kinematics, introduces a nonlinearity in solid mechanics, causing the classic linearised methods to lose their ability to accurately describe the displaced configuration of the structure. When the finite-element method is used, writing the rotation kinematics is also more complex because large rotations in 3D space cannot be represented with a vector. They become in fact non-commutative and must be treated with more complex methods such Euler angles or quaternions (De Soza, 2014). In the present model this only affects the support beam elements (see 3.3), since the rotations of the CABLE elements take place implicitly, following the nodal displacements.
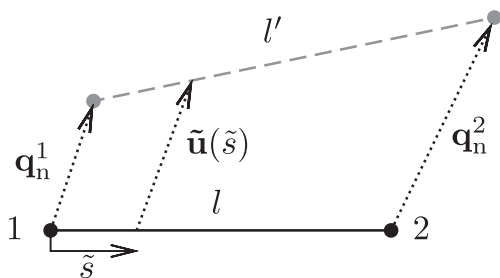
Code_Aster treats large displacements with the updated Lagrangian method (UL) originally introduced by Bathe and Bolourchi (1979), which operates a reactualisation of the structure's geometry at every Newton-Raphson iteration. Contrary to the classic static representation of matrices in linear solid mechanics, the assembled system matrices are continuously recalculated. An example application of the updated Lagrangian method to a 1D element is next given with reference to Fig. 4. The structure's response is represented in the global inertial system of reference, O_{xyz}, whilst the CABLE axial deformation takes place along s in the local frame Ps. We may define the initial, undeformed state of the element with the numeral 0, identifying an initial frame P_{0S0} and an element length l_0. It is then assumed that a new equilibrium must be found for the next instant in time, which is characterised by a different loading state. Let the configuration denoted with '1' be reached after a first Newton-Raphson iteration takes place. The new coordinate s_1 will then be associated to the internal strain of the element in the next iteration, whilst the local deformation is reset to zero as the new configuration with length l_1 becomes the reference geometry. The new reference stress state must naturally be nonzero to account for past strain in the definition of the element's geometric stiffness (De Soza, 2014). The following Newton-Raphson iteration is carried out by recalculating the system tangent matrix in the new configuration, leading to the next displacement guess at 2. The procedure is repeated until convergence is achieved within the time step.

2.3. Seabed contact

The interaction of a mooring line with the seabed is a complex subject which interfaces structural and geotechnical engineering. The state-of-the-art seabed theory proposes a combination of two non-linear dissipative phenomena for the representation of the reactive soil forces: lateral friction and uplift-repenetration resistance (Orcina, 2013). A model of this type is expected to provide a representation of seabed interaction which is accurate enough for the assessment of the fatigue life of mooring segments located around the touchdown point, according to Randolph and Quiggin (2009).

In the present study a smooth and rigid seabed model is used instead, which reduces contact to a reversible conservative phenomenon. Among the contact modelling options available in *Code_Aster*, this is the simplest and most robust. The introduction of dissipative contact is possible in *Code_Aster* and may be sought by further work; this will likely require the creation of shell elements to represent the seabed, and the assignment of
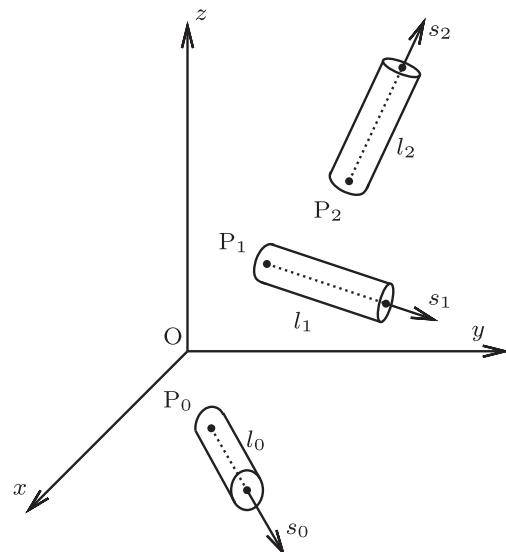

Fig. 3. CABLE element before and after application of nodal displacements.

Fig. 4. Large displacements of 1D element in 3D space. Adapted from Yang and McGuire (1986).

ARTICLE IN PRESS

R. Antonutti et al.
Ocean Engineering xxx (2017) 1–12

a master-slave hierarchy between the mooring line elements and said shells (see the relevant documentation by De Soza, 2015).

Under the current hypotheses, the two variables governing surface contact are d, the clearance between the structure (e.g. a node) and the contact surface, and σ, the normal contact stress. The Hertz-Signorini-Moreau contact conditions are introduced (see for example Yastrebov, 2011):

- Impenetrability (kinematic condition): $d \geq 0$.
- Non-negative contact stress (dynamic cond.): $\sigma \geq 0$.
- Complementarity (energetic condition): $d\sigma = 0$.

The resulting unilateral contact law is then expressed as

$$\begin{cases} d \geq 0 \\ \sigma \geq 0 \\ d\sigma = 0 \end{cases} \tag{3}$$

which is satisfied in the domain visualised in Fig. 5. The positive, semi-definite d-σ relationship found is non-univocal and is not differentiable in $d = \sigma = 0$: these features make it a non-trivial numerical implementation. Unilateral contact is introduced in the model as a constrained optimisation problem using Karush-Kuhn-Tucker (KKT) conditions (Weisstein, 2015), which are in practice applied to an arbitrary set of nodal DoF (Abbas, 2015).

On the user side, the unilateral boundary condition is imposed by applying an analytically defined inequality to the nodal displacements. When touch-down contact over a flat seabed located at $z = -H$ is considered, this assumes the form.

$$\Delta z \geq -(H + z_0). \tag{4}$$

In the above expression Δz denotes the cumulated vertical displacement of a node over the simulation and z_0 its initial vertical coordinate.

2.4. Mooring line hydrodynamics

The Morison approach is employed in the form detailed next to compute the hydrodynamic forces on the lines by taking into account both the structure's motion and the wave kinematics. First, a simplification is made by disregarding the inertial wave forces: due to the small diameter of the mooring lines compared to the length of ocean waves, these are negligible with respect to viscous forces. The same modelling hypothesis is used by commercial mooring simulation software such as aNySIM (MARIN, 2011). The Morison equation term associated to the fluid's added mass force is accounted for in reactive form with the procedure outlined in 2.4.2 and removed from the external loads. This leaves only drag in the Morison equation, which is computed as follows.

The mooring line is assimilated to a circular cylinder of equivalent volume whose diameter is D, the mooring line's volumetric diameter. An arbitrarily oriented orthonormal frame P$\tilde{x}\tilde{y}\tilde{z}$ with $\tilde{x}\equiv s$, is assigned for the decomposition of velocity. Unit vectors $\mathbf{i}$, $\mathbf{j}$, and $\mathbf{k}$ define the directions of
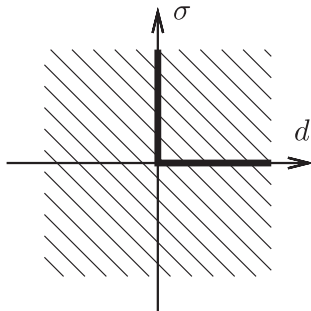

Fig. 5. Unilateral contact law. Thick black lines indicate where this is satisfied.

axes $\tilde{x}$, $\tilde{y}$, and $\tilde{z}$ in the global frame respectively; following from 2.1.1, let $\mathbf{u}$ denote the instantaneous position of a section and $\mathbf{v}$ the absolute flow velocity at the section's location in the fluid, the relative flow velocity is defined by $\mathbf{w} = \mathbf{v} - \dot{\mathbf{u}}$. Subsequently the axial and normal components of vector $\mathbf{w}$ are, with respect to the element's frame,

$$w_{\tilde{x}} = \mathbf{w}\cdot\mathbf{i}, \ w_{\tilde{y}} = \mathbf{w}\cdot\mathbf{j}, \ w_{\tilde{z}} = \mathbf{w}\cdot\mathbf{k}. \tag{5}$$

This enables the decomposition of the drag problem of a porous 1D body in 3D space such as a mooring chain. The axial drag force per unit length is written as

$$\frac{dF_{\tilde{x}}}{dl} = \frac{1}{2}\rho_w c_d^a D \left| w_{\tilde{x}} \right| w_{\tilde{x}}. \tag{6}$$

The transverse component of the relative velocity defined with

$$\mathbf{w}^n = \mathbf{w} - w_x\mathbf{i} \tag{7}$$

enters the computation of the normal drag force:

$$\frac{dF_{\tilde{y}}}{dl} = \frac{1}{2}\rho_w c_d^n D \left| \mathbf{w}^n \right| w_{\tilde{y}}, \ \frac{dF_{\tilde{z}}}{dl} = \frac{1}{2}\rho_w c_d^n D \left| \mathbf{w}^n \right| w_{\tilde{z}}. \tag{8}$$

Note that the axial declination of this formula uses the same reference diameter as the normal one: this is customary in mooring analysis and requires a consistent choice of c_d^a and c_d^n. Equations (6) and (8) can also be written equivalently with reference to the nominal line diameter, which corresponds to the bar diameter for a mooring chain.

2.4.1. Viscous forces

Equations (6) and (8) represent the viscous drag forces, which dominate wave-structure interaction for slender bodies such as mooring lines, and enter the global EoM as a time- and displacement-dependent excitation term. Normal and axial drag forces are treated as distributed loads and their integral over the length of each element is approximated using the Gauss method. Using n Gauss points enables to compute force distributions up to the $(2n - 1)^{th}$ order; in the present application, $n = 3$ is used which should suffice to capture correctly the drag force variability over mooring segments of limited length. In order to do this, the local speed $\dot{\mathbf{u}}$ is calculated at each of the Gauss points by interpolation between the extremity nodes, whilst $\mathbf{v}$ is obtained using the incident wave particle kinematics, providing the local drag force per unit length. The integration of the approximating polynomial times the element shape function finally yields the equivalent nodal forces, which enter the dynamic equilibrium equation after being reexpressed in the global system of reference.

2.4.2. Inertial forces

The inertial fluid reactions may play a significant role in determining a line's dynamic response since they contribute to the effective modal mass. For a standard steel chain, for example, added mass represents about a tenth of the normal modal mass. This is why the reactive part of the inertial hydrodynamic force is considered here by means of a left-hand side (LHS) added mass force. Based on the methods commonly employed by industrial software (e.g. MARIN, 2011; Orcina, 2013), the axial-flow and normal-flow added masses of a slender mooring segment are respectively expressed with

$$m_a^a = c_a^a \rho_w \nabla, \ m_a^n = c_a^n \rho_w \nabla. \tag{9}$$

This formula employs the volumetric acception of the added mass coefficient c_a. The other defining parameters are water density, ρ_w, and the segment volume ∇.

As it will be shown in 3.1, the hydrodynamic added mass is here summed to the mechanical mass of the cables by an increase of material density; this corresponds to assuming $m_a^a = m_a^n = m_a$, which in principle is incorrect. For example, for mooring chains a reasonable normal to

tangential added mass ratio is in the order of 3 (see MARIN, 2011). Fortunately, far from the fairlead excitation the dynamic displacements of pre-tensioned mooring chain segments take place mostly in the transverse direction, reflecting the low modes of a slender and axially stiff structure. It is therefore reasonable to calibrate c_a on the normal added mass at the expense of the representation of axial fluid reaction.

3. Model set-up

Next are presented the user-side procedures which enable to carry out mooring simulations with *Code_Aster*. These start with the selection of an appropriate combination of physical parameters for the simultaneous representation of gravitational, buoyancy, structural inertial, and hydrodynamic added mass forces on the lines. Then the catenary laying procedure is explained, which initialises the mooring simulation. The representation of the floating platform with its rigid-body dynamics is also briefly outlined. Finally, an account is made of the selection of the time integration scheme.

3.1. Chain-equivalent element

In this type of model, Mooring chains need to be assimilated to homogeneous 1D elements. Their complex geometry and the presence of articulated joints (Fig. 6) translate in large longitudinal variations of the mechanical properties at the link scale. In order to correctly represent a mooring chain segment with a bar-type element, these attributes must be expressed in longitudinally averaged form.

A homogeneous CABLE element is defined by the material-specific quantities: E_c and E_c^-, the Young's moduli associated to tension and compression, and the volumetric mass ρ_c. The following geometrical quantities also concur in defining the element: A_c, the element's sectional area, and l_c, its span. Among these parameters, E_c^- is set to zero for a chain (see Orcina, 2013), whilst l_c is dictated by the input mesh for each element. To determine the remaining parameters, the modeller must pay attention to the following aspects:

- *Axial stiffness.* The nominal axial stiffness found in the chain specifications, κ, must be respected by the equivalent cable element, that is $\kappa_c = E_c A_c = \kappa$.
- *Inertial mass per unit length.* Another catalogue parameter is ϱ, the chain's average mass per unit length. In order to assign the correct mass to the equivalent CABLE for the computation of inertial forces, one must satisfy $\rho_m A_c = \varrho$, with ρ_m denoting the chain material's density.

The above relations combined identify the equivalent cable's sectional area and Young's modulus as

$$A_c = \frac{\varrho}{\rho_m}, \quad E_c = \frac{\kappa}{A_c} = \frac{\kappa \rho_m}{\varrho}. \tag{10}$$

Note that the quantities found with Equation (10) must be distinguished from the physical chain's geometric and material properties.

Since in the present implementation the reactive added mass force is approximated with an isotropic increase of inertial mass (see 2.4), an according correction on material density is introduced. Let ρ_w be the water density and c_a the volumetric added mass coefficient, the input equivalent CABLE density becomes
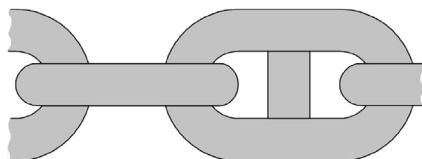

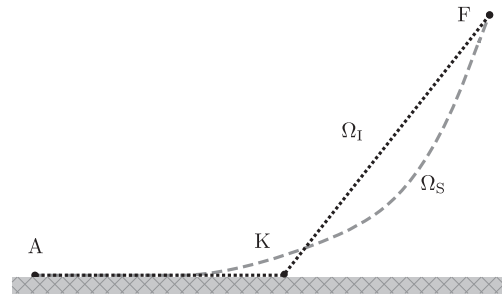**Fig. 6.** Studlink chain geometry.

Fig. 7. Initial controlled geometry before catenary laying (black dots) and target equilibrium geometry (grey dashes).

$$\rho_c = \rho_m + c_a \rho_w. \tag{11}$$

The corrected gravitational acceleration to be applied on the lines in the numerical simulation is obtained with

$$g_c = g \left(1 - \frac{c_a + 1}{c_a + \rho_m/\rho_w} \right), \tag{12}$$

as demonstrated by Antonutti (2015), which insures the representation of the correct weight force per unit length, inclusive of the buoyancy force.

3.2. Catenary laying

Finding the static equilibrium configuration of highly flexible structures such as offshore moorings is a known numerical challenge in finite-element analysis (see for instance Webster, 1980). If one excludes the pre-generation of the equilibrium geometry using catenary formulae, the above translates into finding a gravitationally loaded static equilibrium configuration with *Code_Aster* which is far removed from an arbitrarily chosen initial geometry. The strategy proposed here to solve this problem and initialise the mooring simulation is described next for a single mooring line.

Let F and A be the fairlead and anchor point, whose location in space is known. Assuming L, the unstretched mooring line length, as input, a convenient starting geometry is obtained by breaking the mooring line into two straight segments[2] $\overline{AK}$ and $\overline{KF}$ lying in the vertical plane which contains A and F, with

$$\overline{AK} + \overline{KF} = L. \tag{13}$$

This defines the initial configuration Ω_I shown in Fig. 7. The target static equilibrium configuration Ω_S also appears in the Figure.

From the starting state Ω_I, the quasi-static solver available in *Code_Aster* cannot approach Ω_S through a sequence of quasi-static solutions with increasing excitation, since the equilibrium geometry – neglecting elastic deformation – is the same for any magnitude of the gravitational forcing. In the case of catenary laying the system must find the equilibrium state mostly by rigid-body displacement. Unfortunately, quasi-free rigid-body motion is characterised by a singular tangent stiffness matrix, which makes the problem untractable with the quasi-static solver. In such cases, using the dynamic solver permits to reestablish the equilibrium between internal and external forces thanks to the contribution of inertia (and damping) to the tangent matrix.

Introducing inertia alone stabilises the calculation, but cannot provide the motion decay required to attain Ω_S: a source of dissipation is needed to remove the potential energy differential between Ω_I and Ω_S from the system. This is achieved with the introduction of a controlled

---

[2] Defining the initial mooring line geometry as a set of straight lines in space is functional to both mesh generation and the imposition of the unilateral contact laws of 2.3 in analytical form.

amount of Rayleigh damping. After imposing the gravitational load, clump boundary conditions in F and A, and the seabed contact condition, a decaying dynamic simulation with near-critical damping may be obtained. Such a simulation generally leads to a satisfactory approximation of Ω_S in a few tens of seconds simulation time. At the end, a one-step static simulation is run using Ω_S as input, in order to eliminate any spurious dynamic effect; its output, $\Omega_0 = \Omega(t_0)$, is used to initialise the subsequent simulations of physical interest.

3.3. Floating platform geometry and dynamics

Studying the mechanics of a complete FWT mooring system requires to link the fairlead points to simulate the presence of the floater. A rigid platform model is presently utilised for this sake, which consists in a set of massless, undeformable beam elements (see Fléjou, 2015; for a description of beam elements in *Code_Aster*) each connecting a fairlead to the platform pivoting point.

First, a **motion-driven** approach is proposed: the platform hydromechanics are solved with EDF R&D's time-domain simulator CALHYPSO (see Antonutti et al., 2016; for a description of this software), which provides the six-DoF motion response signals. These are applied within *Code_Aster* as a time-dependent boundary condition located on the platform reference node. In this case the feedback loop between platform dynamics and the dynamic component of the mooring system's response is not represented (see for instance Ormberg and Larsen, 1998). In qualitative terms, the severity of this limitation is proportional to the relative size of the mooring system with respect to the floater, which is governed by water depth (DNV, 2013b; Lin, 2015). The dynamically uncoupled approach used in this study seeks to contain the retroaction inaccuracy through the use of a quasi-static, nonlinear mooring model in CALHYPSO, but cannot include any dynamic mooring retroactions (such as additional dampening of platform motions).

If the platform dynamics are not imposed and need instead to resolved independently by *Code_Aster* in a **coupled simulation**, a rigid hydromechanical floating structure model is introduced in the FE environment. This is done by lumping the aggregate structure mass and hydrostatic stiffness tensors defined at the floating structure's equilibrium, **M** and **K**^{h}, onto a 6-DoF punctual (0D) element (see Fléjou, 2013), where the incident wave excitation $\mathbf{f}(t)$ is also applied. Only harmonic (regular wave) simulations can be organised with this method, since the convolution treatment of aharmonic wave radiation forces is unavailable. By assuming that motion is monochromatic and that its frequency equals that of the incident wave, ω, these forces may be represented in the LHS by assigning frequency-independent, linear added mass and damping tensors to the above defined 0D element, $\mathbf{A}(\omega)$ and $\mathbf{B}(\omega)$, based on the outputs of the frequency-domain radiation calculation.[3] Finally, the hull drag forces are imposed on the structure using an extra set of rigidly connected massless beams and the method of 2.4.1.

Please refer to Section 5 for a definition of the labels used for the different dynamic approaches in the following.

3.4. Numerical damping

Dynamic mooring analyses aim to precisely represent low frequencies (wave excitation and mooring line modes) and tend to be affected by parasitic high-frequency oscillations caused by the system non-linearities. This is a common problem in structural mechanics, often addressed via controlled numerical damping. In particular, Hilber et al. (1977) proposed a dissipative time integration scheme of the Newmark family, commonly referred to as HHT, which introduces low numerical

damping in the low-frequency band and high damping at high frequency, thereby allowing to stabilise the simulation.

For the above reasons, the HHT integration scheme is recommended for the dynamic treatment of CABLE elements in *Code_Aster*, especially in the presence of contact shocks (Fléjou, 2014; Greffet, 2011). In the applications presented in Section 5, a viable value of the numerical damping parameter was chosen by gradually increasing its magnitude until the fairlead tension, the reference output signal, became free of high-frequency noise.

4. Validation cases

Static validation cases for the presented *Code_Aster* workflow are provided by Antonutti (2015). Next, the focus will be placed on dynamic mooring simulation with reference to the DeepCwind-OC4 basin tests. Among the variety of loading cases presented in Masciola et al. (2013), it is here chosen to model the subset for which the authors provide experimental fairlead tension data. This corresponds to six regular wave scenarios (here denoted with letters B to G) plus an irregular wave case. Another low-energy regular wave scenario (A) is reproduced from Coulling et al. (2013). In these tests, wavetrains of varying properties are sent over the structure in the negative X direction (consistently with Fig. 2); this campaign is focussed on highly energetic sea states, representing extreme oceanic conditions, which should help bring out the dynamic features of the mooring system. Tables 1 and 2 define the loading cases considered, using full-scale dimensions.

The regular waves used to excite the structure are moderately steep, causing them to fall into the 2nd order Stokes field of the classic wave theory classification (see Le Méhauté, 1976). A relatively low peak enhancement factor, equalling 2.2, is used in the irregular wave case following the experiments carried out at MARIN.

Note that the intensity of the highest wave conditions considered reaches levels which are typical of 50-year return period oceanic conditions, which are used as the (minimum) ultimate limit state reference by mainstream floating wind standards by ABS (2013), BV (2015), and DNV (2013a).

4.1. Numerical model parameters

The reference study compares experimental and numerical outputs at the full scale, which is also adopted here. The geometric parameters of the OC4 floater (see Fig. 2) are given in Table 3. The aggregated mass and inertia properties of the floating system are provided in Table 4. Since all the considered loading cases feature a parked turbine, which intervenes in the model as a rigid onboard mass, it is not necessary to reproduce the wind turbine particulars in greater detail.

The mooring system geometry is identical to that presented for the full-scale DeepCwind turbine in Robertson et al. (2014), designed for a water depth of 200 m and readily described with the parameters of Table 5. The physical model's mooring chain properties, brought to full scale, are provided with Table 6.

The reported drag coefficients are assigned based on the values proposed by MARIN (2011) for standard (full-scale) chains, whilst the volumetric added mass coefficient is set to unit consistently with

---

[3] For both CALHYPSO and *Code_Aster*, the frequency-domain hydrodynamic data base formed by $|\mathbf{f}|(\omega)$, $\arg(\mathbf{f})(\omega)$, $\mathbf{A}(\omega)$, and $\mathbf{B}(\omega)$ is obtained upfront using NEMOH of the Ecole Centrale de Nantes (see Babarit and Delhommeau, 2015), which solves the linear wave diffraction and radiation problems via the panel method.

Table 1
Regular wave loading cases. Wavelength λ is calculated using the Airy wave dispersion relationship in finite water depth. H_w denotes the wave height and T_w the period.

Case	H_w [m]	T_w [s]	H_w/λ [%]
A	1.92	7.5	2.19
B	7.58	12.1	3.32
C	7.14	14.3	2.24
D	7.57	20.0	1.25
E	10.30	12.1	4.52
F	10.74	14.3	3.37
G	11.12	20.0	1.84

Table 2
Irregular wave loading cases. H_s denotes the significant wave height, T_p the peak period, and $\hat{\gamma} = 2.2$ the peak enhancement factor.

H_s [m]	T_p [s]	Spectrum
7.04	12.18	JONSWAP ($\hat{\gamma} = 2.2$)

Table 3
Geometric properties of the DeepCwind-OC4 floater.

Design draft [m]	20.0
Hull volume [m^3]	13919
Column centre-to-centre spacing [m]	50.0
Diameter of central column [m]	6.5
Diameter of upper offset column [m]	12.0
Diameter of lower offset column [m]	24.0
Height of lower offset column [m]	6.0
Bracing diameter [m]	1.6

Table 4
Global mass and inertia properties of the DeepCwind-OC4 model brought at full scale, moorings excluded.

Displacement [t]	14267
Height of centre of mass from keel [m]	9.792
Central roll/pitch moment of inertia [kg m^2]	$1.344 \cdot 10^{10}$
Central yaw moment of inertia [kg m^2]	$1.396 \cdot 10^{10}$

Masciola et al. (2013).

The gravitational equilibrium requirement is satisfied by countering the undisturbed mooring line weight with an equal vertical force applied at each fairlead. This reintroduces the need to represent the stabilising effect of the mooring system weight with a corresponding gravitational correction in the computation of $\mathbf{K}^h$, which employs a height of the centre of gravity over the keel of 9.743 m.

5. Results and discussion

A comparison of the outputs of the simulations carried out with *Code_Aster* and the MARIN experiments is presented next. The modelling strategies are denoted as follows:

- CALHYPSO. The rigid-body hydromechanical simulation is carried out with the CALHYPSO software, where the mooring forces are calculated with the quasi-static method.
- *Code_Aster* (1). The coupled dynamics of the system are calculated with the dynamic moorings model.
- *Code_Aster* (2A). The platform motions are derived with CALHYPSO as above and subsequently imposed to the dynamic moorings model (motion-driven simulation).
- *Code_Aster* (2B). Equivalent to *Code_Aster* (2A), neglecting the incident wave kinematics in the calculation of mooring drag forces.

For regular waves, both the motion and the fairlead tension outputs are given in the response amplitude operator form (RAO), using the maxima and minima of the steady-state response signal. Whereas this is in principle a linear dynamic analysis procedure, it is here extended to represent the range of oscillation of cyclical outputs. In this context it should be noted that whilst motion signals closely follow sinusoidal

Table 5
Geometry of the DeepCwind-OC4 mooring system, consisting of three chains with 120° spacing.

Fairlead depth below the free surface [m]	14.00
Fairlead radius from platform centre [m]	40.87
Anchor radius from platform centre [m]	837.6
Unstretched line length L [m]	835.5

Table 6
Parameters of the studless chain used to moor the DeepCwind-OC4 model, brought at full scale. Drag coefficients are referred to the chain's nominal diameter.

Nominal diameter [m]	0.0766
Material density ρ_m [kg/m^3]	8500
Mass per unit length ϱ [kg/m]	123.5
Axial stiffness κ [N]	753.6×10^6
Volumetric added mass coefficient c_a [−]	1.0
Axial drag coefficient c_d^a [−]	0.8
Normal drag coefficient c_d^n [−]	2.4

waveforms, mooring tensions exhibit significant distortion.

Where irregular waves are concerned, the power spectral density (PSD) of the quantities of interest is presented. This is calculated for a stationary regime of 2-h duration. Provided that the highest natural period of the structure, that of surge motion, is in the order of 100 s, more than 50 resonant surge cycles are allowed. Considering this feature, and that the input energy is located at smaller periods, 2 h seem sufficient to capture the variability of the stochastic processes involved.

5.1. Regular waves

Fig. 8 displays the platform's dynamic response under regular wave excitation found by the UMaine MARIN campaign, and through the simulations carried out with CALHYPSO and the coupled dynamic model.

In-plane motions (surge, heave, pitch) are the only rigid-body DoF excited.

As commonly found in slack-moored offshore structures, **surge** amplitude increases with the oscillation period. Similar response operators are found for the two different wave heights examined. In this DoF, the outputs of CALHYPSO and *Code_Aster* are close to equivalent, showing the limited effect of mooring dynamics on platform motion in this particular case. With reference to the experiments, both models tend to underestimate response slightly, especially for $T_w = 20$ s where the error is in the order of 10%. A similar accuracy has been obtained in the reference study by modelling these cases with NREL's FAST (Coulling et al., 2013).

The normalised dynamic response in **heave** is limited to a fraction of a unit at low periods, whilst at the near-resonant period of $T_w = 20$ s it exceeds unit. The heave DoF is also well predicted by both numerical models, which produce amplitude errors of a few percent points. It is once again at 20 s that the models err the most, showing however better performance than the FAST results reported by Coulling et al. (2013). This may be explained by the explicit formulation of platform drag in the present models, taking into account the wave kinematics. This significantly contributes to exciting the structure vertically, which does not happen in the referenced FAST simulation where the drag model is only reactive. Said thesis is reinforced by the model-to-model comparison provided by Masciola et al. (2013).

Pitch appears to be a more problematic DoF to be simulated in this case. CALHYPSO mostly underestimates pitch response across the studied range, with an error pattern closely resembling that of the simulation outputs published by Coulling et al. (2013). In all cases but A and B, the explicit inclusion of mooring dynamics enabled by *Code_Aster* seems to positively affect the accuracy of the simulated platform response. Once again, the system dynamics at the wave period of $T_w = 20$ s appear to be particularly sensitive to the modelling approach. For pitch, this is likely to be an effect of the proximity of the semi-submersible platform's excitation suppression point, which reduces the effect on response of the inertial wave excitation, dominant elsewhere, thereby exalting the importance of secondary hydrodynamic force systems.

The measured and predicted **fairlead tensions** in regular waves are shown in Fig. 9. A first and most striking, if unsurprising, observation is that the quasi-static representation of CALHYPSO severely underestimates the tension variance across the entire set of cases. All dynamic mooring model outputs provide a more accurate estimate of the
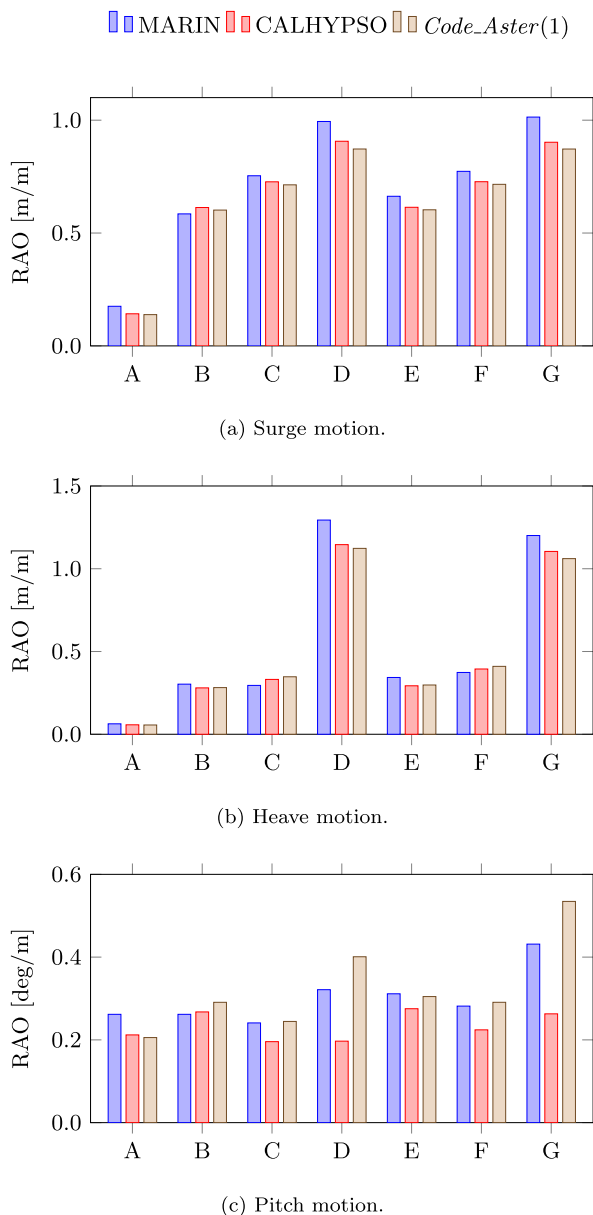
(a) Surge motion.

(b) Heave motion.

(c) Pitch motion.

Fig. 8. Measured and computed motion response amplitude operator of the DeepCwind-OC4 floating system in regular waves. The experimental data are digitised from Coulling et al. (2013).

(a) Line tension at fairlead F1.

(b) Line tension at fairlead F2.

Fig. 9. Measured and computed fairlead tension response amplitude operator in regular waves. The experimental data are digitised from Coulling et al. (2013).

tension RAOs, both for the upwave fairlead F1 and the downwave fairlead F2, and exceed the performance of the dynamic mooring simulations presented in Masciola et al. (2013), which underpredict the response amplitude. The best performance is provided by the coupled dynamic simulation, 'Code_Aster (1)', with the exception of downwave tension at 20 s (D, G) which is better predicted by the motion-driven approach. Accuracy seems to deteriorate for larger wave heights, as observable from period-matched case pairs such as B, E. The root cause may be sought in the extra tuning required by the chain drag coefficients (governing the dynamic mooring effects at high energy), which are currently static and calibrated at the full scale. Another possible cause may be the absence of potential, 2nd order hydrodynamic excitation (wave drift forces) in the present numerical models.

The three dynamic modelling approaches presented exhibit good mutual agreement with the exception of the downwave line tension for $T_w = 20$ s. In this case the coupled simulation provides a tension RAO which is around 75%–80% of the motion-driven one, possibly due to the differing pitch responses obtained by CALHYPSO and Code_Aster (1), as
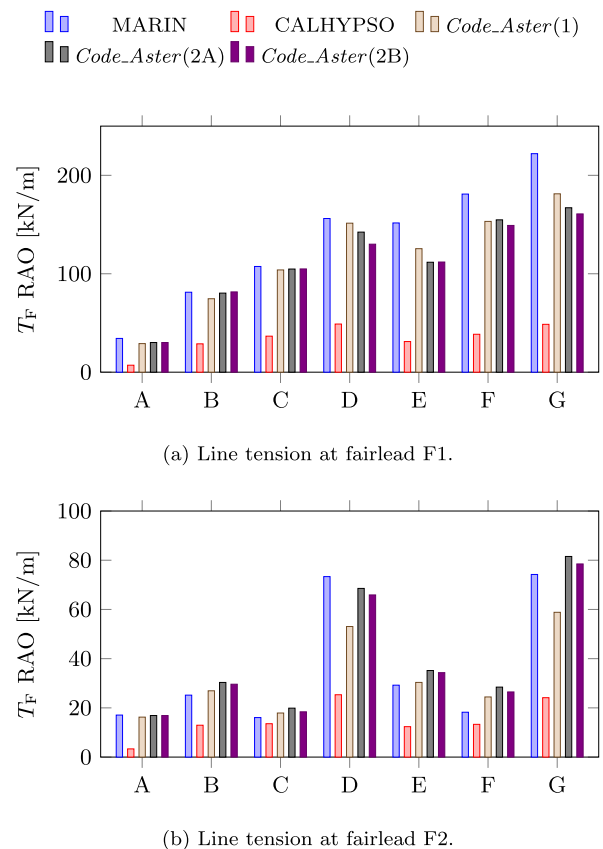
already seen in Fig. 8c. Further work will be required to clarify the system's dynamics at this particularly sensitive period.

The motion-driven output tensions obtained by neglecting the incident wave kinematics are shown to slightly undershoot the standard motion-driven results – by up to 8% in the worst case. This result is used to justify the use of approach 'Code_Aster (2B)' in the following to simulate the mooring dynamics under irregular waves (irregular wave kinematics are not implemented in Code_Aster yet).

Finally, in terms of impact of modelling choices on mooring design, it is worth noticing that for this particular floating system the quasi-static approach severely underestimates tension ranges virtually in all wave conditions from low-energy (more frequent) to high-energy (less frequent). This underscores the need for dynamic mooring simulation for robust mooring line dimensioning for both fatigue and ultimate limit states.

5.2. Irregular waves

CALHYPSO is used here to compute the DeepCwind FWT motion response under the irregular wave case defined in Table 2. Verifying the correct prediction of its dynamic response features is a required passage before tackling the analysis of the dynamic fairlead tensions obtained with Code_Aster. In order to facilitate the interpretation of the output spectra, the uncoupled natural frequencies of the floater and of the undisturbed mooring lines are provided in Table 7. The latter are calculated with the method described in Wilson (2003), based on the transverse-excitation modes of offshore mooring lines, and disregarding the hydrodynamic added mass.

The PSD of motion in the three excited DoF is provided with Fig. 10, where the experimental results are available only for the translational DoF.

The **surge** motion spectrum is bimodal, with two distinct response

ARTICLE IN PRESS

R. Antonutti et al.   Ocean Engineering xxx (2017) 1–12

Table 7
Natural frequencies of the floating DeepCwind-OC4 system.

Subsystem	Mode	Frequency [Hz]
Platform	Surge/sway	0.009
Platform	Heave	0.059
Platform	Roll/pitch	0.039
Platform	Yaw	0.012
Mooring lines	1st transverse	0.077
Mooring lines	2nd transverse	0.153
Mooring lines	3rd transverse	0.230

peaks descending from the first-order and second-order (drag) hydrodynamic excitation on the platform; both peaks exhibit good agreement with the measurements. It is important to remark that satisfactory resonant response in surge is here obtained numerically without the inclusion of potential-flow, difference-frequency forces. As it was also observed during the VALEF2 project, the representation of hull drag forces on a position-updated basis introduces a low-frequency forcing which can dominate the excitation of the surge mode, depending on the type of structure studied. In light of this, the underprediction of resonant response in surge by the numerical model utilised in Masciola et al. (2013) may be due to the missing actualisation of the Morison elements following the platform's displacements.

Heave response in the wave frequency band is also well represented by the numerical model, whilst the adjacent peak which identifies resonant motion – excited by both inertial and viscous wave forces – is slightly less well captured: whilst the excess motion amplitude may be due to insufficient vertical dissipation in the model, the slight natural frequency mismatch is likely due to the numerical added mass deficit on the platform's slender elements, modelled with the Morison approach.

Using the motion time histories as input, the motion-driven simulation performed with the 'Code_Aster (2B)' method provides the **fairlead tension** spectra displayed in Fig. 11. Only the experimental spectrum of the upwave fairlead is available for comparison.

Both spectra are trimodal, with a low-frequency peak governed by the resonant surge response of the platform, a broader wave frequency peak and a high-frequency tail. The dynamically simulated spectrum matches the experimental observations, net of the spectral noise caused at high frequency by the constant block averaging resolution chosen for the post-processing. Mainly due to the angled geometry of the downwave mooring lines with respect to the in-plane motion of the platform, the dynamic component of the simulated tension is much lower than in the upwave line.

An important limitation of the present comparison consists in the random phases chosen to translate the input wave spectrum into a time-domain signal. A more rigorous numerical representation of the experiments could be carried out by matching the basin test phases; unfortunately, these are unknown. Whilst the first-order dynamic response is unaffected by phasing, response related to nonlinear processes combining different harmonics is linked to the specific phase set in the realisation (see for instance Roald et al., 2013). Due to missing information regarding the spectral realisation of the basin tests (phases and duration of experiment), the phasing issue is not addressed in the present study.

In terms of tension prediction, the performance of the quasi-static moorings model included in CALHYPSO is satisfactory only at low frequency. In the wave frequency band and above this model severely underestimates the tension range, especially at the upwave fairlead. This is an expected outcome of the use of the quasi-static catenary representation of mooring forces in a highly dynamic simulation. Although the first natural mode of the mooring lines sits in the vicinity of the first-order excitation peak, a sensitivity analysis (not included) permitted to determine that drag rather then inertia is the dominant process causing tension magnification in this band, which is not captured with the quasi-static approach. This is a known feature of catenary mooring systems in limited water depth.
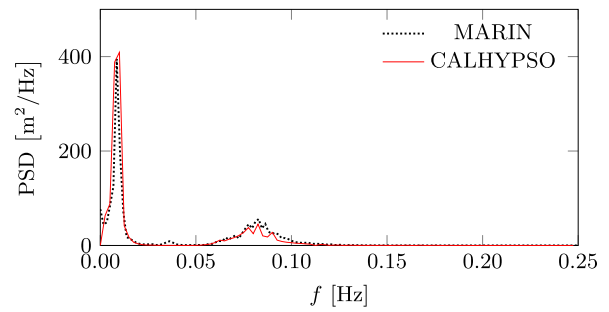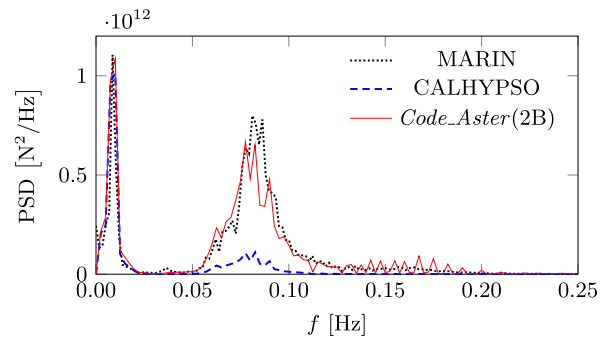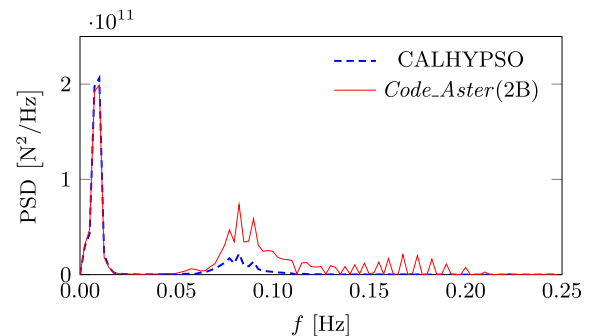

(a) Surge motion.
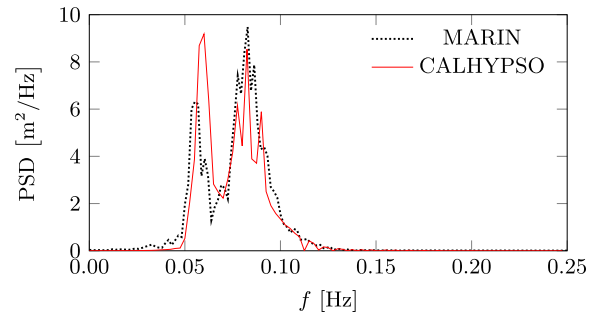
(b) Heave motion.

Fig. 10. Measured and computed power spectral density of the motions of the DeepCwind-OC4 turbine in irregular waves. The experimental curves are digitally imported from Masciola et al. (2013).

(a) Line tension at fairlead 1.

(b) Line tension at fairlead 2.

Fig. 11. Measured and computed power spectral density of the fairlead tensions under irregular wave excitation. The experimental curve is digitally imported from Masciola et al. (2013).

Both tension spectra obtained with *Code_Aster* contain significant high-frequency energy, due to the mechanical nonlinearities of the mooring system and a possible excitation of the second transverse mode

of the lines (see Table 7). This prediction is confirmed by the available experimental spectrum. The broad frequency spreading of this response feature may be explained with the parametric line behaviour related to the low-frequency variation of tension and suspended length caused by platform motion.

6. Conclusion and further work

For the first time *Code_Aster*, the open-source mechanical analysis software developed by EDF R&D, has been used to simulate offshore mooring dynamics. A successful application to the floating wind technology is included in the present work. After the presentation of the methodological choices, hinging on the 1D finite-element representation of slender and compliant structures and unilateral contact, it has been shown that appropriate model set-up and initialisation permit to handle the hydromechanics of catenary moorings with this general-purpose tool.

A range of dynamic simulations has been performed and compared with experimental results available in the literature. The model has been shown to satisfactorily predict the coupled platform-moorings dynamics of a FWT in regular waves. In particular, the dynamic fairlead tensions are well represented, albeit with seemingly decreasing accuracy as the wave height is increased. A motion-driven simulation has also been carried out, representing the system's dynamics under irregular waves, and compared with experimental observations from the literature. Once again the fairlead tensions are correctly predicted by *Code_Aster*. The computational cost of the presented method is relatively moderate, as a high-energy 2-h sea state takes six to 7 h to run on a desktop machine.

It has been shown that all the constituents of dynamic tension response (low-frequency, wave frequency, and high-frequency) are captured by the numerical solution, suggesting that the model correctly reproduces the main physical processes at play on the lines. Accuracy may be improved by further work: for instance, additional calibration efforts may be sought in the future, perhaps by complementing the modelling workflow with reduced-scale analyses.

A side observation can also be made based on the comparison of the experiments with the different numerical models employed: nonlinear mooring line hydrodynamics (drag) govern the fairlead tension variance, most dramatically so in high-energy sea states. In these conditions a quasi-static model cannot even predict the correct order of magnitude of the tension oscillations, as already pointed out in the past by authors (e.g. Hall and Goupee (2015)) dealing with the same case study. Unlike in conventional floating offshore applications, dynamic (or at least drag-augmented quasi-static) mooring analysis seems to be strictly necessary to produce a reliable floating wind system design.

A more thorough verification of the capabilities of the *Code_Aster* model will require the evaluation of the behaviour of different platform and mooring system combinations, especially considering that the presented case uses a relatively large floater concept with a conventional slack mooring system. Considering the current trends in FWT technology, priority may be placed on the implementation of fibre rope behaviour (especially with respect to nonlinear stiffness characteristics) and on the verification of taut/tensioned system simulation. The implementation of higher-order wave forcing on the platform in the calculation chain should also permit to ascertain their influence on the system's dynamic response, especially considering that the low-frequency motions and tensions obtained here seem to match the experiments although no second-order potential hydrodynamics are represented. A further step may consist in dynamically linking the finite-element solver to CALHYPSO to enable fully coupled mechanical simulations. In the future, platform hydro-elasticity may also be treated using this approach.

The inclusion of turbine loads, already possible with the motion-driven approach, should be used for further investigations. These will provide key insights on the frequency ranges excited in fully characterised operational states, where turbine thrust drives platform offset and hence the peak mooring tensions. Also, the cyclical loading from the turbine is expected to bear a minor impact on mooring line fatigue.

In its current form, the presented *Code_Aster*-based dynamic moorings model has become part of EDF R&D offshore mechanics calculation chain and has already been used for concept verification and classification; it has been employed by the utility to evaluate FWT mooring arrangements of different complexity, in the context of the Group's calls for tenders – where solutions by MODEC, IDEOL, and other applicants were analysed – and of joint industry project Vertiwind. Further developments may be directed toward coefficient calibration, a more detailed representation of the seabed interaction and of the fluid-structure interaction, and a generalisation of the types of mooring components tractable (ropes, buoys, etc.). In particular, finite elements of higher complexity (beams) may be used for the representation of less flexible 1D equipment such as umbilical cables, provided that a reliable large-displacement behaviour be implemented.

Once the remaining building blocks of the presented aero-hydro-mooring model will be in place and validated, standard mooring verification cycles may be run: line tension maxima detected over the entire DLC set will be compared with the minimum breaking loads of the lines to verify the compliance of any configuration with the standards; rainfall counting post-treatment routines will enable fatigue life estimates on the basis of suitable reduced load case lists.

References

Abbas, M., 2015. Formulation discrète du contact-frottement. Code_Aster documentation R5.03.50. http://www.code-aster.org/V2/doc/default/fr/man_r/r5/r5.03.50.pdf.

ABS, 2013. Guide for Building and Classing Floating Offshore Wind Turbine Installations. Tech. Rep. DNV-OS-J103. American Bureau of Shipping.

Antonutti, R., 2015. Numerical Study of Floating Wind Turbines: Hydro- and Aero-mechanics. Ph.D. thesis. The University of Edinburgh, Edinburgh, Scotland, UK.

Antonutti, R., Peyrard, C., Johanning, L., Incecik, A., Ingram, D., 2016. The effects of wind-induced inclination on the dynamics of semi-submersible floating wind turbines in the time domain. Renew. Energy 88, 83–94. http://www.sciencedirect.com/science/article/pii/S0960148115304389.

Babarit, A., Delhommeau, G., 2015. Theoretical and numerical aspects of the open source BEM solver NEMOH. In: Proc. 11th European Wave and Tidal Energy Conference. Nantes, France.

Bachynski, E.E., Etemaddar, M., Kvittem, M.I., Luan, C., Moan, T., 2013. Dynamic analysis of floating wind turbines during pitch actuator fault, grid loss, and shutdown. Energy Procedia 35, 210–222. http://www.sciencedirect.com/science/article/pii/S1876610213012605.

Bae, Y.H., Kim, M.H., 2013. Rotor-floater-tether coupled dynamics including second-order sum–frequency wave loads for a mono-column-TLP-type FOWT (floating offshore wind turbine). Ocean. Eng. 61, 109–122. http://www.sciencedirect.com/science/article/pii/S0029801813000255.

Bathe, K.-J., Bolourchi, S., 1979. Large displacement analysis of three-dimensional beam structures. Int. J. Numer. Methods Eng. 14 (7), 961–986. http://web.mit.edu/kjb/www/Publications_Prior_to_1998/Large_Displacement_Analysis_of_Three-Dimensional_Beam_Structures.pdf.

Borg, M., Collu, M., Brennan, F.P., 2012. Offshore floating vertical axis wind turbines: advantages, disadvantages, and dynamics modelling state of the art. In: Proc. RINA Marine & Offshore Renewable Energy International Conference. RINA, London, UK, pp. 33–46.

BV, 2015. Classification and Certification of Floating Offshore Wind Turbines. Tech. Rep. NI 572 DT R01 E, Bureau Veritas.

CAELinux, Jul. 2015. Doc:Code-Aster - CAELinuxWiki. Online. http://caelinux.org/wiki/index.php/Doc:Code-Aster. http://caelinux.org/wiki/index.php/Doc:Code-Aster.

Castro-Santos, L., Gonzales, S.F., Diaz-Casas, V., 2013. Mooring for floating offshore renewable energy platforms classification. In: Proc. International Conference on Renewable Energies and Power Quality. Bilbao, Spain. http://icrepq.com/icrepq%2713/277-castro.pdf.

Chakrabarti, S., 2005. Handbook of Offshore Engineering, vol. 2. Elsevier, Oxford, UK.

Cheng, Z., Wang, K., Gao, Z., Moan, T., 2015. Dynamic modelling and analysis of three floating wind turbine concepts with vertical axis rotor. In: Proc. 25th International Offshore and Polar Engineering Conference. Kona, HI, USA. https://www.onepetro.org/conference-paper/ISOPE-I-15-172.

Coulling, A.J., Goupee, A.J., Robertson, A.N., Jonkman, J.M., Dagher, H.J., 2013. Validation of a FAST semi-submersible floating wind turbine numerical model with DeepCwind test data. J. Renew. Sustain. Energy 5 (2).

de Boom, W., 2011. Floating supports for offshore wind: small structures – big challenges. In: Proc. 30th International Conference on Ocean, Offshore and Arctic Engineering (Rotterdam, The Netherlands).

De Soza, T., 2014. Poutres multi-fibres en grands déplacements. Code_Aster documentation R3.08.09.

De Soza, T., 2015. Opérateur DEFI_CONTACT. Code_Aster Documentation U4.44.11. http://www.code-aster.org/V2/doc/default/fr/man_u/u4/u4.44.11.pdf.

DNV, 2013a. Design of Floating Wind Turbine Structures. Tech. Rep. DNV-OS-J103, Det Norske Veritas.

DNV, 2013b. Position Mooring. Tech. Rep. DNV-OS-E301, Det Norske Veritas. https://exchange.dnv.com/publishing/codes/docs/2013-10/OS-E301.pdf.

EDF, 2014. Code Aster: Analysis of Structures and Thermomechanics for Studies & Research. EDF R&D. http://www.code-aster.org/V2/UPLOAD/DOC/Presentation/plaquette_aster_en.pdf.

Fléjou, J.-L., 2013. Modélisations DIS_T et DIS_TR. Code_Aster documentation U3.11.02. http://www.code-aster.org/V2/doc/default/fr/man_u/u3/u3.11.02.pdf.

Fléjou, J.-L., 2014. Modélisation des câbles. Code_Aster documentation R3.08.02. http://www.code-aster.org/V2/doc/default/fr/man_r/r5/r5.03.40.pdf.

Fléjou, J.-L., 2015. Éléments "exacts" de poutres (droites et courbes). Code_Aster documentation R3.08.01. http://www.code-aster.org/V2/doc/default/fr/man_r/r3/r3.08.01.pdf.

Goupee, A.J., Fowler, M.J., Kimball, R.W., Helder, J., de Ridder, E.-J., 2014. Additional Wind/wave basin testing of the DeepCwind semi-submersible with a performance-matched wind turbine. In: Proc. ASME 2014 33rd International Conference on Ocean, Offshore and Arctic Engineering. American Society of Mechanical Engineers.

Greffet, N., 2011. Algorithme Non Linéaire Dynamique. Code_Aster Documentation R5.05.05. http://www.code-aster.org/V2/doc/default/fr/man_r/r5/r5.05.05.pdf.

Hall, M., Buckham, B., Crawford, C., Nicoll, R.S., 2011. The importance of mooring line model fidelity in floating wind turbine simulations. In: Proc. OCEANS. Waikoloa, HI, USA. http://ieeexplore.ieee.org/xpls/abs_all.jsp?arnumber=6107138.

Hall, M., Goupee, A., 2015. Validation of a lumped-mass mooring line model with DeepCwind semisubmersible model test data. Ocean. Eng. 104, 590–603. http://www.sciencedirect.com/science/article/pii/S0029801815002279.

Hilber, H.M., Hughes, T.J.R., Taylor, R.L., 1977. Improved numerical dissipation for time integration algorithms in structural dynamics. Earthq. Eng. Struct. Dyn. 5 (3), 283–292. http://onlinelibrary.wiley.com/doi/10.1002/eqe.4290050306/abstract.

Jeon, S.H., Cho, Y.U., Seo, M.W., Cho, J.R., Jeong, W.B., Nov. 2013. Dynamic response of floating substructure of spar-type offshore wind turbine with catenary mooring cables. Ocean. Eng. 72, 356–364.

Johanning, L., Smith, G.H., Wolfram, J., 2007. Measurements of static and dynamic mooring line damping and their importance for floating WEC devices. Ocean. Eng. 34 (14–15), 1918–1934. http://linkinghub.elsevier.com/retrieve/pii/S0029801807001126.

Jonkman, J., Larsen, T., Hansen, A., Nygaard, T., Maus, K., Karimirad, M., Gao, Z., Moan, T., Fylling, I., Nichols, J., Kohlmeier, M., Pascual Vergara, J., Merino, D., Shi, W., Park, H., 2010. Offshore Code Comparison Collaboration within IEA Wind task 23: phase IV results regarding floating wind turbine modeling. In: Proc. European Wind Energy Conference. Warsaw, Poland. http://www.nrel.gov/docs/fy14osti/60600.pdf.

Kallesoe, B.S., Paulsen, U.S., Kohler, A., Hansen, C.H., 2011. Aero-hydro-elastic response of a floating platform supporting several wind turbines. In: Proc. 49th AIAA Aerospace Sciences Meeting. Orlando, FL, USA. http://arc.aiaa.org/doi/pdf/10.2514/6.2011-721.

Karimirad, M., 2013. Modeling aspects of a floating wind turbine for coupled wave–wind-induced dynamic analyses. Renew. Energy 53, 299–305. http://www.sciencedirect.com/science/article/pii/S0960148112007616.

Kim, H.C., Jang, H.K., Kim, M.H., Bee, Y.H., 2015. Coupled dynamic analysis of a MUFOWT with transient broken-blade incident. In: Proc. 25th International Offshore and Polar Engineering Conference. Kona, HI, USA. https://www.onepetro.org/conference-paper/ISOPE-I-15-617.

Koo, B., Goupee, A., Lambrakos, K., Lim, H.-J., 2014. Model test data correlations with fully coupled hull/mooring analysis for a floating wind turbine on a semi-submersible platform. In: 33rd International Conference on Ocean, Offshore and Arctic Engineering. San Francisco, CA, USA. In: http://proceedings.asmedigitalcollection.asme.org/data/Conferences/ASMEP/81076/V09BT09A034-OMAE2014-24254.pdf.

Le Méhauté, B., 1976. An Introduction to Hydrodynamics and Water Waves. Springer-Verlag, New York, USA.

Lin, Z., 2015. A Hydrodynamic Analysis of Deep-water Moorings. Ph.D. thesis. University of Strathclyde, Glasgow, Scotland, UK.

MARIN, 2011. aNySIM Documantation - Mooring. Tech. rep. https://wiki.marin.nl/images/2/2d/MOORING.pdf.

Masciola, M., Jonkman, J., Robertson, A., 2014. Extending the capabilities of the Mooring Analysis Program: a survey of dynamic mooring line theories for integration into FAST. In: Proc. 33rd International Conference on Ocean, Offshore and Arctic Engineering. San Francisco, CA, USA. In: http://proceedings.asmedigitalcollection.asme.org/proceeding.aspx?articleid=1912167.

Masciola, M., Robertson, A., Jonkman, J., Coulling, A., Goupee, A., 2013. Assessment of the importance of mooring dynamics on the global response of the deepcwind floating semisubmersible offshore wind turbine. In: Proc. 23rd International Offshore and Polar Engineering Conference. Anchorage, Alaska, USA.

Matha, D., Fechter, U., Kühn, M., 2011. Non-linear multi-body mooring system model for floating offshore wind turbines. In: Proc. OFFSHORE2011. Amsterdam, The Netherlands.

Mavrakos, S.A., Papazoglou, V.J., Triantafyllou, M.S., Hatjigeorgiou, J., 1996. Deep water mooring dynamics. Mar. Struct. 9 (2), 181–209.

Muskulus, M., 2011. Designing the next generation of computational codes for wind-turbine simulations. In: Proc. 21st International Offshore and Polar Engineering Conference. Vol. 318. Maui, HI, USA. http://e-book.lib.sjtu.edu.cn/isope2011/data/papers/11TPC-1005Musku.pdf.

Orcina, 2013. OrcaFlex Manual Version 9.7a. Tech. rep., Orcina Ltd. http://www.orcina.com/SoftwareProducts/OrcaFlex/Documentation/OrcaFlex.pdf.

Ormberg, H., Larsen, K., 1998. Coupled analysis of floater motion and mooring dynamics for a turret-moored ship. Appl. Ocean Res. 20 (1), 55–67.

Randolph, M., Quiggin, P., 2009. Non-linear hysteretic seabed model for catenary pipeline contact. In: 28th International Conference on Ocean, Offshore and Arctic Engineering. Honolulu, HI, USA, pp. 145–154. In: http://proceedings.asmedigitalcollection.asme.org/proceeding.aspx?articleid=1623566.

Roald, L., Jonkman, J., Robertson, A., Chokani, N., 2013. The effect of second-order hydrodynamics on floating offshore wind turbines. Energy Procedia 35, 253–264. http://www.sciencedirect.com/science/article/pii/S1876610213012642.

Robertson, A., Jonkman, J., Masciola, M., Song, H., 2014. Definition of the Semisubmersible Floating System for Phase II of OC4. Tech. Rep. NREL/TP-5000–60601. National Renewable Energy Laboratory.

Stendal, L.C., 2015. Analysis Methods for Mooring Systems with Focus on Accidental Limit State. M.Sc. thesis. Norwegian University of Science and Technology, Trondheim, Norway.

Thakore, D.A., 2014a. Finite Element Analysis Using Open Source Software, second ed. Moonish Enterprises, Brisbane, Australia.

Thakore, D.A., 2014b. Intermediate Finite Element Analysis Using Open Source Software, first ed. Moonish Enterprises, Brisbane, Australia.

Vryhof, 2010. Anchor Manual 2010. Vryhof Anchors. http://www.vryhof.com/pdf/anchor_manual.pdf.

Webster, R.L., 1980. On the static analysis of structures with strong geometric nonlinearity. Comput. Struct. 11 (1–2), 137–145. http://www.sciencedirect.com/science/article/pii/0045794980901534.

Weisstein, E.W., Jul. 2015. Kuhn-Tucker Theorem. Online. http://mathworld.wolfram.com/Kuhn-TuckerTheorem.html. http://mathworld.wolfram.com/Kuhn-TuckerTheorem.html.

Wilson, J.F., 2003. Dynamics of Offshore Structures. John Wiley & Sons, Hoboken, NJ, USA.

Yang, Y.-B., McGuire, W., 1986. Joint rotation and geometric nonlinear analysis. J. Struct. Eng. 112 (4), 879–905. https://doi.org/10.1061/(ASCE)0733-9445(1986)112:4(879).

Yastrebov, V., 2011. Computational Contact Mechanics: Geometry, Detection and Numerical Techniques. Ph.D. thesis. Mines ParisTech, Paris, France. http://www.yastrebov.fr/DOCs/VA_Yastrebov_PhD_thesis.pdf.

Zhang, R., Tang, Y., Hu, J., Ruan, S., Chen, C., 2013. Dynamic response in frequency and time domains of a floating foundation for offshore wind turbines. Ocean. Eng. 60, 115–123. http://www.sciencedirect.com/science/article/pii/S0029801812004246.